PROCEEDINGS, Twenty-Fifth Workshop on Geothermal Reservoir Engineering
Stanford University, Stanford, California, January 24-26, 2000
SGP-TR-165

LBNL-44802

MODELING OF PHASE-PARTITIONING TRACERS IN FRACTURED RESERVOIRS

K. Pruess*, M.J. O'Sullivan#, and B.M. Kennedy*

* Earth Sciences Division, Lawrence Berkeley National Laboratory, Berkeley, CA 94720
# Department of Engineering Science, The University of Auckland, Auckland, New Zealand
e-mail: K_Pruess@lbl.gov

ABSTRACT

This paper presents modeling concepts and illustrative simulations for the migration of phase-partitioning tracers in boiling two-phase reservoirs. The mathematical model implemented in the TOUGH2 simulator is reviewed. Migration of artificial and natural (noble gas) tracers is simulated for production-injection scenarios under vapor-dominated conditions. Simulated trends reflect an interplay of different reservoir processes and conditions, and compare favorably with observations at The Geysers reservoir.

INTRODUCTION

Natural and artificial tracers can provide very useful information on geothermal fluid flows and reservoir processes. For applications in two-phase and vapor-dominated reservoirs, there is increasing interest in tracers that partition between liquid and gas phases (Adams, 1995). Examples include naturally occurring noble gases and other non-condensible gases, such as CO_2 and CH_4, as well as a variety of man-made chemicals, such as halogenated hydrocarbons. Because of their phase-partitioning properties, these tracers can not only identify preferential flow paths, but they can also be used to monitor reservoir processes and conditions, including in-place water saturation, and the vaporization of injected water (Giggenbach, 1980; d'Amore and Pruess, 1986).

In this paper we are interested in "gas-like" tracers, whose phase partitioning can be described by Henry's law

$$P_\kappa = K_h x_l^\kappa \tag{1}$$

Here, P_κ is the partial pressure of tracer κ in the gas phase, x_l^κ is the mol fraction dissolved in the liquid phase, and K_h is the Henry's coefficient, which has units of pressure and is a function of temperature.

We briefly review the processes that affect tracer migration under multiphase conditions, and discuss special issues that arise in finite difference modeling of multiphase diffusion. Numerical simulations are presented for tracer migration in vapor-dominated systems subject to fluid production and injection.

TRACER TRANSPORT

Migration of phase-partitioning tracers occurs by multiphase advection, hydrodynamic dispersion, and diffusion in gas and liquid phases; it may also be affected by sorption and decay. Here we summarize transport processes as modeled by the TOUGH2 geothermal reservoir simulator (Pruess et al., 1999).

Advection

In a multiphase system, the advective flux of a mass component κ is given by

$$\mathbf{F}^\kappa\Big|_{adv} = \sum_\beta X_\beta^\kappa \mathbf{F}_\beta \tag{2}$$

where X_β^κ is the mass fraction of component κ in phase β (= liq, gas), and $\mathbf{F}_\beta$ is the mass flux in phase β, given by a multiphase extension of Darcy's law that includes relative permeability and capillary pressure effects.

Molecular Diffusion

The flux due to molecular diffusion is usually written as being proportional to the gradient in the concentration of the diffusing component (Fick's law). For single-phase conditions diffusive flux is (Bird et al., 1960)

$$\mathbf{f} = -d\nabla C \tag{3}$$

where d is an effective diffusivity, which in general depends on properties of the diffusing species, the pore fluid, and the porous medium. The concentration variable C may be chosen in a number of different ways (mass per unit volume, moles per unit volume, mass or mol fraction, etc.; Bird et al., 1960; de Marsily, 1986). The Fickian diffusion model is attractive because of its simplicity, but it is not generally valid for gases. Fortunately, the more accurate "dusty gas" model (Mason and Malinauskas, 1983; Webb, 1998) can be shown to reduce to Fick's law for trace gases present in small concentrations (Webb and Pruess, 2000).

For general two-phase conditions, the total diffusive mass flux of a trace component κ can be written as a sum of the fluxes in liquid and gas phases, as follows

$$\mathbf{f}^{\kappa} \quad = \quad -\Sigma_l^{\kappa} \nabla X_l^{\kappa} - \Sigma_g^{\kappa} \nabla X_g^{\kappa} \qquad (4),$$

where

$$\Sigma_\beta^\kappa \quad = \quad \phi \tau_0 \tau_\beta \rho_\beta d_\beta^\kappa \qquad (5)$$

is the effective diffusive strength coefficient in phase β. Here, ϕ is porosity, $\tau_0\tau_\beta$ is the tortuosity which includes a porous medium dependent factor τ_0 and a saturation-dependent factor $\tau_\beta = \tau_\beta(S_\beta)$ that is akin to relative permeability, ρ_β is density, and d_β^κ is the diffusion coefficient of component κ in bulk fluid phase β, which is a function of fluid pressure and temperature.

At typical geothermal reservoir conditions of T = 240 ˚C, P = $P_{sat}(T)$ = 33.48 bar, gas diffusivities are of order 10^{-6} m^2/s, similar to thermal diffusivities of common geothermal reservoir rocks. Porous medium tortuosity factors may range from 0.4 for highly permeable media, such as sands or fractures, to 0.01 for tight matrix rocks with permeabilities in the microdarcy range (Kreamer et al., 1988; Webb and Pruess, 2000). Liquid phase diffusivities are typically three to four orders of magnitude smaller than those in the gas phase. The small values for effective diffusivities suggest that diffusive transport distances will be small during the time periods of interest in geothermal reservoir development. Rough estimates indicate that the length scale for diffusive penetration in the gas phase will be of order 20 m over the productive lifetime of a geothermal reservoir (30 years). This will be negligible wherever advective transport is significant, as e.g. for flow in fractures. However, diffusion may play an important role in fracture-matrix exchange (see below).

Space discretization of diffusive flux in multiphase conditions raises some subtle issues. For tracers that are both water-soluble and volatile, diffusive fluxes in gas and liquid phases are strongly coupled by phase partitioning effects, and it is not possible to evaluate these fluxes separately. TOUGH2 uses a scheme where the entire multiphase diffusive flux is written as the product of a single mass fraction gradient and a single effective strength coefficient (Pruess et al., 1999). This formulation was shown to cope well even with the worst case scenario of diffusion across a sharp gas-water interface.

Hydrodynamic Dispersion

Hydrodynamic dispersion arises from an interplay between non-uniform advection and molecular diffusion in porous media that have heterogeneities on multiple scales. It is usually modeled in analogy to Fickian diffusion. Much hydrogeological research during the last twenty years has shown the diffusive analogy to be of limited validity and usefulness for field problems; yet for many applications there are no practical alternatives. A "standard" approach to hydrodynamic dispersion, with appropriate generalization to multiphase flow systems, has been incorporated in TOUGH2. Dispersive mass flux is written

$$\mathbf{F}^{\kappa}\Big|_{dis} \quad = \quad -\sum_\beta \rho_\beta \overline{\mathbf{D}}_\beta \nabla X_\beta^\kappa \qquad (6)$$

where $\mathbf{D}_\beta$ is the hydrodynamic dispersion tensor (de Marsily, 1986; Oldenburg and Pruess, 1995).

FIVE-SPOT PRODUCTION-INJECTION SYSTEM

This problem was designed to capture reservoir conditions and processes relevant to The Geysers vapor-dominated reservoir. To simplify the simulation problem we take advantage of symmetries, and assume that production and injection wells are arranged in a regular five-spot pattern (see Fig. 1). A single layer of 500 m thickness is modeled, and a 5-point parallel grid of 196 square blocks with 10.88 m length is used to represent a 1/8 symmetry element. Problem specifications as given in Table 1 are similar to what was used in earlier work on production-injection behavior in the Southeast Geysers (Pruess and Enedy, 1993), and in field-wide modeling of The Geysers (Williamson, 1992). The reservoir is assumed fractured with an average fracture spacing of 50 m, and is modeled with the method of multiple interacting continua ("MINC;" Pruess and Narasimhan, 1985). Production and injection occurs at a constant rate of 16 kg/s (full well basis). Injection enthalpy is 125 kJ/kg, corresponding to a temperature of injected water of approximately 29.8 ˚C. R134a and tritium tracers are injected as pulses of 8 hour duration at concentrations of 100 ppm, corresponding to a total amount of 46.08 kg for each of the tracers. Both R134a (chemically, $C_2H_2F_4$) and tritiated water have been successfully used in tracer tests at The Geysers (Beall et al., 1994, 1998).

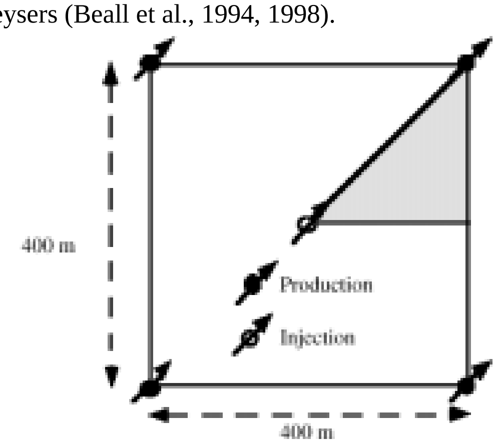

Figure 1. Five-spot well pattern, with shading showing a 1/8 symmetry element.

Two variations were explored. Case 1 has large water saturation in the rock matrix, corresponding to a reservoir zone that has seen very little depletion, while Case 2 has small water saturation, corresponding to a strongly depleted region. These cases are intended to represent in a general way the Bear Canyon and SMUD regions at The Geysers, respectively, for which tracer tests were reported by Beall et al. (1994, 1998), although no attempt was made to reproduce site parameters in specific detail. For Case 1, tracer injection is preceded by a 30-day period of injection-production without tracers. Simulated breakthrough curves for the two cases are shown in Fig. 2 on linear and logarithmic scales.

Table 1. Specifications of Five-spot Problem

Reservoir properties	
Average permeability (of fracture network)	43.2×10^{-15} m^2
Matrix permeability	1.9×10^{-18} m^2
Fracture porosity	1 %
Matrix porosity	3 %
Thickness	500 m
Permeability-thickness	21.6×10^{-12} m^3
Fracture spacing	50 m
Relative permeability liquid: van Genuchten (1980); parameters gas: Corey (1954); parameter	 $\lambda = .4438$; $S_{lr} = .08$ $S_{gr} = .05$
Capillary pressure van Genuchten (1980); parameters	 $\lambda = .4438$; $S_{lr} = 0$; $P_0 = 3238$ Pa (fractures); 17.27×10^5 Pa (matrix)
Pattern area	160,000 m^2 (= 39.5 acres)
Well spacing (distance from injector to producer)	282.8 m (928.0 ft)
Production/injection rate (full well basis)	16 kg/s
Injection enthalpy	125 kJ/kg
Gridding	
5-point parallel grid, spacing	10.88 m
Initial conditions	
Pressure	33.479 bar
Temperature	240 ˚C
Water saturation in fractures	0.0001
in matrix	0.99 (Case 1) 0.068 (Case 2)
Tracer injection	
R134a	8 hours at 100 ppm
Tritium	8 hours at 100 ppm

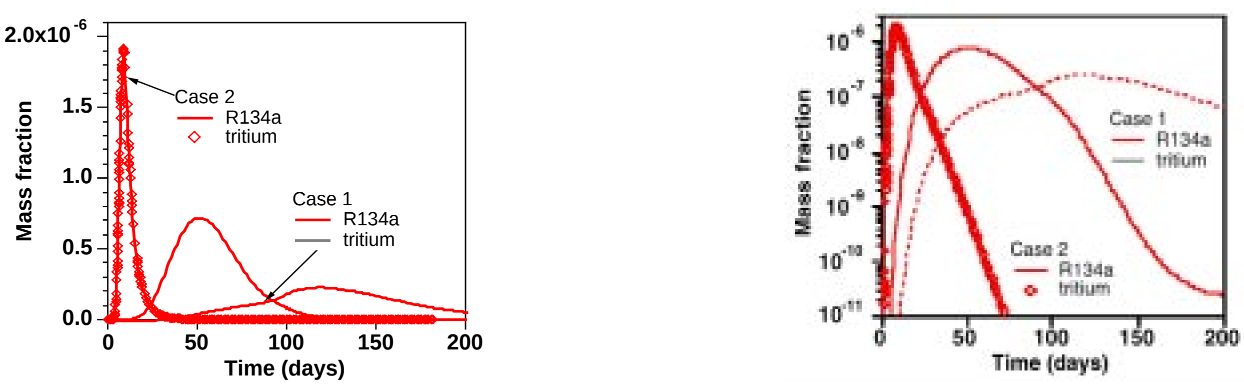

Figure 2. Simulated tracer breakthrough curves for five-spot problem in a vapor-dominated reservoir on linear scale (left) and log scale (right). Case 1 corresponds to conditions with large water saturation in the rock matrix, while Case 2 corresponds to a depleted reservoir zone with small water saturation.

For the undepleted reservoir (Case 1), R134a breaks through earlier and at higher concentrations than tritium. This is explained by the partial vaporization of injected fluid, and the preferential partitioning of the volatile R134a into the vapor phase. At T = 240 ˚C the viscosity of saturated vapor is a factor 6.5 less than that of saturated liquid. Therefore, for the same pressure gradients, vapor will flow at 6.5 times larger velocity than liquid. Tritium partitions evenly between liquid and gas phases, so that it is subject to more attenuation and retardation from liquid-gas phase partitioning than R134a. For strongly depleted reservoir conditions (Case 2), all of the injected fluid is quickly completely vaporized, and breakthrough curves for R134a and tritium are virtually identical. Note that, because of the symmetry of the five-spot problem, simulated tracer concentrations correspond to a situation in which tracer would be injected simultaneously into all injection wells. If only one injection well receives tracer, while the remaining three wells in the basic pattern receive untraced water, all produced tracer concentrations would be reduced by a factor 4.

The timing and trends of simulated tracer breakthrough agree remarkably well with field observations by Beall et al. (1994, 1998), supporting their interpretations of the underlying reservoir mechanisms. For depleted conditions, as in the SMUD region of The Geysers that was tested by Beall et al. (1994), tracer returns show a sharp peak after a few days. For undepleted conditions, a broad distribution is obtained with a maximum at about 50 days, similar to results obtained by Beall et al. (1994) for the Bear Canyon region of The Geysers. However, there are significant discrepancies in the magnitude of produced tracer concentrations, which are indicative of reservoir conditions and processes that are not captured in our simulation. For example, peak concentrations observed by Beall et al. (1994) for the depleted case ranged from 0.1 ppm to as high as 10 ppm, as compared to 2 ppm in our simulation (0.5 ppm if concentrations are scaled down by a factor 4, to allow for symmetry). The large concentrations seen in the field test provide clear evidence for non-volume averaged flow along localized preferential pathways. For undepleted reservoir conditions, peak tracer concentrations observed by Beall et al. (1994) were less than .005 ppm in all production wells, while our simulation gave much higher values of approximately 0.2 ppm (allowing for a factor 4 reduction from symmetry). A possible explanation for the low concentrations seen in the field could be that under conditions of slow and partial vaporization (Case 1), much of the injected fluid migrates by gravity force to greater depth. This three-dimensional effect is not captured in our single-layer model.

Table 3. Data for Noble Gas Isotopes

In our simulations, tracer recovery is actually larger for the undepleted system (Case 1; see Table 2). This occurs because in Case 1 virtually all traced fluid remains in the fractures, while in the depleted system (Case 2) a considerable fraction of the tracer enters the rock matrix along with the overall advective flow.

Table 2. Tracer Recovery after 300 Days.

tracer	R134a	tritium
Case 1	45.18 kg (98.1 %)	33.31 kg (72.3 %)
Case 2	19.94 kg (43.3 %)	20.62 kg (44.7 %)
Case 2 w/diffusion	23.14 kg (50.2 %)	20.85 kg (45.2 %)

The simulations discussed so far neglect diffusive transport. Another simulation was performed in which diffusion was included. For gas phase diffusivity of R134a, we used data applicable to similar chemicals, namely, $d_{g0} = 1.7 \times 10^{-5}$ m^2/s at standard conditions of $P_0 = 10^5$ Pa, $T_0 = 0$ ˚C, and a temperature exponent of $\theta = 1.78$ (Vargaftik, 1975). This corresponds to a gas diffusivity at in situ conditions of $d_g^* = d_{g0}^* (P_0/P)\left((T+273.15)/273.15\right)^\theta = 1.56 \times 10^{-6}$ m^2/s. Aqueous phase diffusivity was taken as 1.7×10^{-9} m^2/s. A tortuosity factor of $\tau_0 = 0.01$ was used, appropriate for tight matrix rocks with permeability in the microdarcy range (Webb and Pruess, 2000). Simulation results presented in Fig. 3 show that diffusion can be a significant mechanisms for fracture-matrix exchange, giving rise to long tails in the breakthrough curve. Considerably stronger tails would arise for fracture spacing smaller than the D = 50 m assumed here.

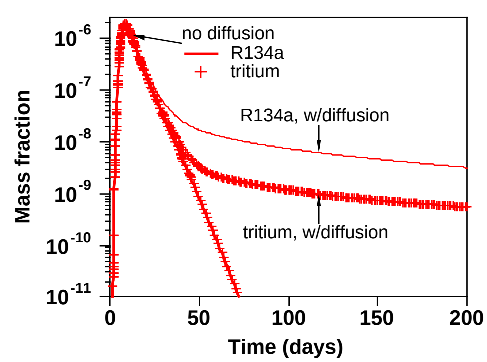

Figure 3. Breakthrough curves for Case 2, showing effects of diffusive mass exchange between fractures and matrix.

NOBLE GASES

Noble gases are present in atmospheric air in concentrations that are well known. Waters in contact with atmospheric air will dissolve noble gases in

Isotope	Partial pressure in air, Pa	Dissolved mass fraction in water at T = 10 ˚C	Henry's coefficient, Pa T = 10 ˚C	Henry's coefficient, Pa T = 240 ˚C	Diffusion coefficient in saturated water vapor at T = 240 ˚C, m^2/s
22Ne	0.170	2.440e-11	8.510e9	3.197e9	2.884e-6
36Ar	3.184	2.134e-9	2.981e9	2.729e9	1.739e-6
84Kr	0.0658	1.990e-10	1.542e9	2.542e9	1.326e-6
132Xe	2.370e-3	2.142e-11	8.110e8	1.977e9	1.073e-6

concentrations that depend on the respective Henry's law coefficients (Table 3). With the exception of helium and 40Ar, which occur in magmatic gases and are also generated through U, Th, and K decay in the crust, the isotopically stable noble gases have no significant subsurface sinks or sources. These gases make excellent tracers because (1) they are chemically inert and (2) their abundance can be measured by mass spectroscopy with exquisite precision. Solubilities of noble gases in water are a function of temperature and increase with molecular weight of the gas (Crovetto et al., 1982; Smith and Kennedy, 1983). Observed relative abundances of noble gases in subsurface waters are affected by the temperatures at which recharge occurred, and by phase partitioning in multiphase systems. If phase-partitioning effects are absent, relative abundances of noble gases in groundwaters can be used to make inferences about past terrestrial climates (e.g. Ballentine and Hall, 1999). If boiling occurs, the noble gases will preferentially partition into the gas phase, more so for the less soluble lighter gases. Thus, the vapor will be enriched in light noble gases, while the residual liquid will have a higher relative abundance of the heavier ones. These effects suggest that noble gases may be useful tracers for phase change processes in geothermal reservoirs.

In the simulations presented below, mass fractions of noble gases in the aqueous phase were initialized at the values corresponding to dissolved mass fractions in water of T = 10 ˚C in dissolution equilibrium with atmospheric gases (see Table 3). This corresponds to a physical picture in which waters are assumed to retain their original noble gas inventory during the evolution of the reservoir. That is, phase separation processes that could alter the noble gas content during the natural evolution of a geothermal system have been neglected.

Block Depletion

This problem considers uniform depletion of a zero-dimensional reservoir, with initial conditions of T = 240 ˚C, P = $P_{sat}(T)$ = 33.479 bar, S_g = 0.01. Initial noble gas mass fractions correspond to dissolution equilibrium with atmospheric air at T = 10 ˚C (see Table 3). Depletion is simulated by withdrawing fluid at a constant rate, using small time steps in the early period when noble gas concentrations change rapidly. Liquid phase is assumed immobile, so that only single-phase vapor is produced. Fig. 4 shows mass fractions of 22Ne and 132Xe in produced vapor as a function of reservoir depletion, along with the Xe:Ne ratio. Produced Xe mass fraction is a factor 0.5429 smaller than Ne mass fraction initially, reflecting the smaller Henry's constant of Xe at 240 ˚C, as well as the somewhat smaller initial dissolved Xe mass fraction. As the reservoir is being depleted, noble gas concentrations decline rapidly due to the preferential partitioning into the gas phase which leaves behind gas-depleted liquid. Depletion of only 0.62 % of original fluid reserves removes 91 % of original Ne inventory, and 84 % of original Xe inventory. The Ne mass fraction drops more rapidly because it more strongly fractionates into the gas phase, and the Xe:Ne ratio goes to large values as depletion proceeds.

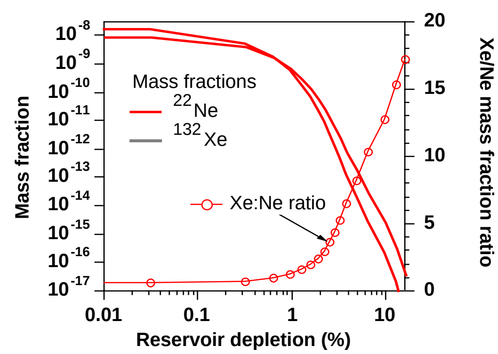

Figure 4. Simulated noble gas concentrations for production from a 0-D vapor-dominated reservoir.

Radial Flow

1-D radial flow to a well was simulated for the same reservoir conditions as for the five-spot problem (Table 1), except that a single homogeneous porous medium was used instead of a fractured reservoir description. Initial noble gas concentrations were set at the values corresponding to surface waters at T = 10 ˚C. A central well produces at a constant rate of 20 kg/s. Results for Neon and Xenon mass fractions are shown in Fig. 5 for cylindrically shaped reservoirs with 10^3 and 10^4 m radius, respectively. For the time scale of the simulation, the R = 10^4 m reservoir is infinite acting. Produced mass fractions are seen to go through a modest decline at early time, then stabilize at constant values. Finite-size effects for the R = 10^3 m reservoir are seen to come into play after about 2 years (6.3e7 s), leading to a rapid depletion of remaining nobel gas inventory. The stabilization of mass fractions and mass fraction ratios (Fig. 6) for the infinite-acting system is a consequence of a similarity property: thermodynamic conditions in the reservoir depend upon time t and distance R only through the similarity variable $\xi = R^2/t$ (O'Sullivan, 1981). Mass fractions of non-condensible gases can be shown to approach a constant as ξ --> 0, corresponding to t --> .

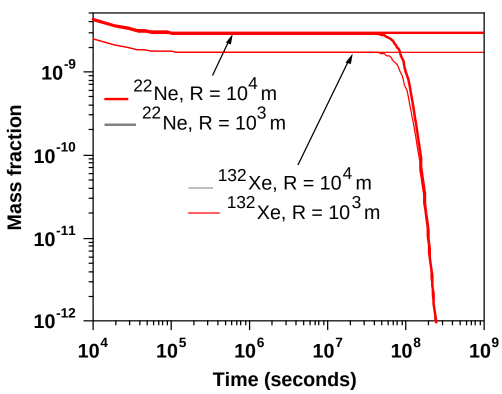

Figure 5. Produced noble gas mass fractions for 1-D cylindrical reservoirs.

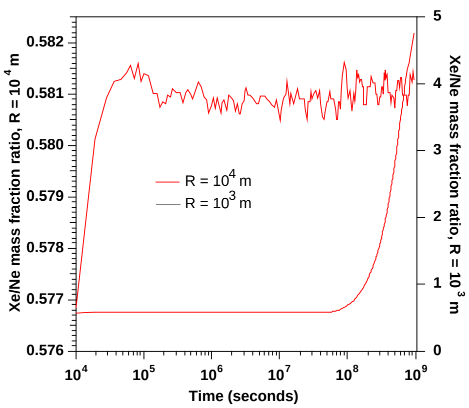

Figure 6. Xe:Ne mass fraction ratios for cylindrical reservoirs.

CONCLUSIONS

The migration of water-soluble and volatile tracers in fractured two-phase reservoirs occurs through a complex interplay of processes on different space and time scales.

Interwell tracer transport is dominated by advective flow. In fractured reservoirs, tracer returns can be strongly affected by diffusive exchange with matrix rocks of low intrinsic permeability.

Phase-partitioning tracers show promise not only for the identification of preferential flow paths, but also as tools for monitoring reservoir processes, such as boiling of injected water.

Numerical simulation capabilities for phase-partitioning tracers can be used for design and analysis of tracer tests.

ACKNOWLEDGEMENT

The first author acknowledges helpful discussions with Curt Oldenburg, Yu-Shu Wu, and Steve Webb. Thanks are due to Kenzi Karasaki and Stefan Finsterle for a review of the manuscript and the suggestion of improvements. This work was supported by the Assistant Secretary for Energy Efficiency and Renewable Energy, Office of Geothermal and Wind Technologies, of the U.S. Department of Energy under Contract No. DE-AC03-76SF00098.

REFERENCES

Adams, M. (1995), Vapor, Liquid, and Two-Phase Tracers for Geothermal Systems. *Proceedings, World Geothermal Congress 1995*, pp. 1875-1880, International Geothermal Association.

Ballentine, C.J. and C.M. Hall (1999), Determining Paleotemperature and other Variables by using an Error-weighted, Non-linear Inversion of Noble Gas Concentrations in Water, *Geochim. Cosmochim. Acta*, Vol. 63, No. 16, pp. 2315 - 2336.

Beall, J.J., M.C. Adams and P.N. Hirtz (1994), R-13 Tracing of Injection in The Geysers, *Transactions*, Geothermal Resources Council, Vol. 18, pp. 151 - 159.

Beall, J.J., M.C. Adams and P.N. Hirtz (1998), Evaluation of R134a as an Injection Water Tracer in the Southeast Geysers, *Transactions*, Geothermal Resources Council, Vol. 22, pp. 569 - 573.

Bird, R., W.E. Stewart and E.N. Lightfoot (1960), *Transport Phenomena*, John Wiley & Sons, New York, NY.

Corey, A.T. (1954), The Interrelation Between Gas and Oil Relative Permeabilities, *Producers Monthly*, pp. 38 - 41.

Crovetto, R., R. Fernandez-Prini and M.L. Japas (1982), Solubility of Inert Gases and Methane in H_2O and D_2O in the Temperature Range of 300 to 600 K, *J. Chem. Phys.*, Vol. 76, No. 2, pp. 1077 - 1086.

d'Amore, F. and K. Pruess (1986), Correlations Between Stream Saturation, Fluid Composition and Well Decline in Vapor-Dominated Reservoir, *Geothermics*, Vol. 15, No. 2, pp. 167-183.

de Marsily, G. (1986), *Quantitative Hydrogeology*, Academic Press, Orlando, FL.

Giggenbach, W. F. (1980), Geothermal Gas Equilibria, *Geochim. Cosmochim. Acta*, Vol. 44, pp. 2021 - 2032.

Kreamer, D.K., E.P. Weeks and G.M. Thompson (1988), A Field Technique to Measure the Tortuosity and Sorption-Affected Porosity for Gaseous Diffusion of Materials in the Unsaturated Zone with Experimental Results from near Barnwell, South Carolina, *Water Resour. Res.*, Vol. 24, No. 3, pp. 331 - 341.

Mason, E.A. and A.P. Malinauskas (1983), *Gas Transport in Porous Media: The Dusty Gas Model*, Elsevier, Amsterdam, The Netherlands.

Oldenburg, C.M. and K. Pruess (1995), Dispersive Transport Dynamics in a Strongly Coupled Groundwater-Brine Flow System. *Water Resour. Res.*, Vol. 31, No. 2, pp. 289 - 302.

O'Sullivan, M.J. (1981), A Similarity Method for Geothermal Well Test Analysis, *Water Resour. Res.*, Vol. 17, No. 2, pp. 390 – 398.

Pruess, K., C. Oldenburg and G. Moridis (1999), TOUGH2 User's Guide, Version 2.0, Lawrence Berkeley National Laboratory Report LBNL-43134, Berkeley, CA.

Pruess, K. and S. Enedy (1993), Numerical Modeling of Injection Experiments at The Geysers, Proceedings, 18th Workshop on Geothermal Reservoir Engineering, pp. 63 - 71, Stanford University, Stanford, CA.

Pruess, K. and T.N. Narasimhan (1985), A Practical Method for Modeling Fluid and Heat Flow in Fractured Porous Media, *Soc. Pet. Eng. J.*, 25 (1), 14-26.

Smith, S.P. and B.M. Kennedy (1983), The Solubility of Noble Gases in Water and in NaCl Brine, *Geochim. Cosmochim. Acta*, Vol. 47, pp. 503 - 515.

van Genuchten, M.Th. (1980), A Closed-Form Equation for Predicting the Hydraulic Conductivity of Unsaturated Soils, *Soil Sci. Soc. Am. J.*, Vol. 44, pp. 892 - 898.

Vargaftik, N.B. (1975), *Tables on the Thermophysical Properties of Liquids and Gases*, 2nd Ed., John Wiley & Sons, New York, NY.

Webb, S.W. (1998), Gas-Phase Diffusion in Porous Media - Evaluation of an Advective-Dispersive Formulation and the Dusty Gas Model for Binary Mixtures, *J. Por. Media*, Vol. 1, No. 2, pp. 187 - 199.

Webb, S.W. and K. Pruess. Evaluation of Fick's Law for Trace Gas Diffusion in Porous Media, to be submitted to *Water Resour. Res.*, 2000.

Williamson, K.H. (1992), Development of a Reservoir Model for The Geysers Geothermal Field, in: C. Stone, (ed.), *Monograph on the Geysers Geothermal Field*, Special Report No. 17, pp. 179 - 187, Geothermal Resources Council, Davis, CA.